Proceedings of the 5th World Congress on Momentum, Heat and Mass Transfer (MHMT'20)
~~Lisbon, Portugal~~ Virtual Conferences – October, 2020
Paper No. ICMFHT 185
DOI: 10.11159/icmfht20.185

CFD-based Characterization of the Single-use Bioreactor Xcellerex™ XDR-10 for Cell Culture Process Optimization

Diana Kreitmayer[1,2], Srikanth Gopireddy[2], Tomomi Matsuura[3], Shizuka Kondo[3], Hirofumi Kakihara[3], Koichi Nonaka[3], Nora Urbanetz[2], Eva Gutheil[1]

[1]Interdisciplinary Center for Scientific Computing (IWR), Heidelberg University
Im Neuenheimer Feld 205, Heidelberg, Germany
diana.kreitmayer@iwr.uni-heidelberg.de; gutheil@iwr.uni-heidelberg.de
[2] Pharmaceutical Development, Daiichi-Sankyo Europe GmbH
Luitpoldstraße 1, Pfaffenhofen (Ilm), Germany
[3] Biotechnology Research Laboratories, Biologics Division, Daiichi-Sankyo Co. Ltd.
2716-1Kurakake, Akaiwa, Chiyoda-machi, Ohra-dun, 370-0503, Japan

Abstract – The Xcellerex™ XDR-10 is a cylindrical stirred tank single-use bioreactor with a flat bottom and a maximum working volume of 10 L. Computational fluid dynamics (CFD) simulations with both Euler-Euler and Euler-Lagrange approaches are used to characterize the hydrodynamic conditions inside the vessel for different operating conditions. They include the full range of recommended working volume (4.5 L to 10 L), impeller speeds from 40 rpm to 360 rpm, and sparging rates from 0.02 L/min to 0.5 L/min. The evaluated parameters include the specific oxygen mass transfer coefficient (k_La), mixing time, vortex formation, energy dissipation rate, and shear stress. To evaluate the experimentally observed vortex formation the change in agitated liquid height is measured and used for validation. Additionally, k_La and mixing time are determined experimentally and used for validation. The lowest mixing time and a high k_La are observed at the maximum stirrer speed with both approaches as well as in experiments. However, analysis of the volume-average energy dissipation rate for this condition violates the upper limit of 0.4 m^2/s^3, which has been observed to have negative impact on mammalian cell culture performance. This indicates that, while a high stirrer speed seems recommendable to improve oxygen transfer and reduce mixing time, going up to the maximum level will lead to high hydrodynamic stress on the cultivated cells and should be avoided. The present study shows how CFD can provide in-depth understanding of a bioreactor with non-standard geometry. Furthermore, despite their differences, both modeling approaches lead to similar results and perform similarly well with respect to experimental validation. Thus, for the considered operating conditions the effect of bubbles on the liquid flow, which is mainly driven by the mechanical agitation of the stirrer, is small and the computationally less expensive one-way coupled Euler-Lagrange approach can characterize the process well.

Keywords**:** Euler-Lagrange simulation, Euler-Euler simulation, OpenFOAM, Single-use bioreactor, Xcellerex™ XDR-10, Mixing time, Oxygen mass transfer coefficient, Vortex formation

1. Introduction

Single-use bioreactors have become popular because of their lower initial investment cost and reduced down time between cultivation runs [1]. However, their geometry significantly deviates from classical stainless-steel reactors. A very significant difference is that they are usually not equipped with baffles. For this new type of geometry and the resulting effect on bioreactor hydrodynamics, there is less experience in optimization of operating conditions. Therefore, the characterization of the hydrodynamics with Computational Fluid Dynamics (CFD) can be useful to tackle this problem [2]. The Xcellerex™ XDR-10 is a cylindrical single use bioreactor with a flat bottom, a central bottom mounted stirrer, and the maximum working volume is 10 L. Homogenization is achieved by the rotational motion of the stirrer, and oxygen transfer to the cultivation medium is achieved by sparging air or oxygen through a microporous sparger at the bottom. Two different spargers with a pore size of 2 μm and 20 μm are available. Consequently, the flow type can be described as a mechanically agitated liquid flow with rising disperse bubbles.

When two different phases must be considered such as a continuous liquid and a disperse bubble phase, several established modeling approaches exist including the Volume of Fluids, Euler-Lagrange, and the Euler-Euler approaches.

Here, the capabilities of the Euler-Lagrange approach, where discrete bubbles are tracked, and the Euler-Euler approach, which tracks both the gas and liquid phases based on their volume fractions, are compared. In the one-way coupled Euler-Lagrange approach the effect of bubbles on the liquid phase is neglected while in the Euler-Euler approach momentum transfer from the gas-phase to the liquid-phase is considered. Simulations for eight different operating conditions, representing a screening Design of Experiments, are performed with each method and compared against experimental data for mixing time and specific oxygen mass transfer coefficient (k_La). Furthermore, the liquid velocity, the bubble trajectories, and the vortex formation are analyzed for both methods. Additionally, the risk of cell damage due to hydrodynamic stress is analyzed using the average turbulent energy dissipation rate [3] and the maximum shear stress [4, 5].

2. Methods

This section provides a brief overview of the selected test conditions as well as the experimental and numerical methods.

2.1. Test Conditions

The operating conditions considered in both experiments and simulations are based on a screening Design of Experiments, which is given in Table 1. The culture medium liquid properties measured at room temperature are a density ρ of 1,010.8 kg/m^3 and a viscosity of 0.001126 Pa s. In simulations temperature is assumed to be 37°C which is typical for cell culture processes. For the 2 μm sparger a bubble size of 0.8 mm is assumed and for the 20 μm sparger a bubble size of 1 mm is assumed.

Table 1: Tested operating conditions following a screening Design of Experiments with condition 4 as the center point.

Condition	Working volume (L)	Stirrer speed (rpm)	Sparging rate (L/min)	Sparger pore size (μm)
1	4.5	100	0.25	2
2	10	100	0.25	2
3	7	100	0.02	2
4	7	100	0.25	2
5	7	100	0.50	2
6	7	100	0.25	20
7	7	40	0.25	2
8	7	360	0.25	2

2.2. Experimental Methods

Mixing time measurements are performed with the iodine de-colorization method [6]. The reactor content is colorized by adding 8 mL/L starch solution (10 g/L soluble starch and 2 g/L benzoic acid) and 0.1 mL/L iodine solution (400 g/L potassium iodine and 127 g/L iodine). Addition of 0.1 mL/L thiosulfate tracer (166 g/L 1N sodium thiosulfate) leads to decolorization. The mixing time is taken with a stop watch as the time from tracer addition to complete decolorization.

The specific oxygen mass transfer coefficient k_La is measured with the dynamic method [7]. After depleting the oxygen from the liquid by sparging with nitrogen, the oxygen sparging is switched back on. The value of k_La is determined from the slope of the temporal evolution of the natural logarithm of the dissolved oxygen concentration

$$\ln\left(\frac{\mathbf{DO}^* - \mathbf{DO}(t)}{\mathbf{DO}^* - \mathbf{DO}(t_0)}\right) = -k_L a(t - t_0) \tag{1}$$

where DO* is the saturation concentration, DO(t_0) is the initial concentration and DO(t) is the concentration at time t and t_0 is the initial time.

The change in liquid height due to sparging and stirring for all conditions is analyzed by measuring the difference in liquid height with a ruler before stirring and sparging is started and again after stable process conditions are reached.

2.3. Numerical Methods

One-way coupled Euler-Lagrange simulations are performed with MixIT [8] and momentum transfer from the bubbles to the liquid is not considered. The liquid flow is described with the incompressible Reynolds-averaged Navier-Stokes equations using the standard *k*-*ε* model

$$\nabla \mathbf{u} = 0 \tag{2}$$

$$\frac{\partial \mathbf{u}}{\partial t} + \nabla(\mathbf{u}\mathbf{u}) = -\nabla p + \nabla\left(v_{\text{eff}}\left(\nabla \mathbf{u} + \nabla \mathbf{u}^{\text{T}} - \frac{2}{3}\mathbf{I}\nabla \mathbf{u}\right) - \frac{2}{3}\mathbf{I}k\right) \tag{3}$$

$$\frac{\partial k}{\partial t} + \nabla(k\mathbf{u}) = \nabla\left(\left(\nu + \frac{\nu_{\text{t}}}{\sigma_k}\right)\nabla k\right) + G_k - \varepsilon \tag{4}$$

$$\frac{\partial \varepsilon}{\partial t} + \nabla(\varepsilon\mathbf{u}) = \nabla\left(\left(\nu + \frac{\nu_{\text{t}}}{\sigma_\varepsilon}\right)\nabla \varepsilon\right) + C_{1\varepsilon}\frac{\varepsilon}{k}G_k - C_{2\varepsilon}\frac{\varepsilon^2}{k} \tag{5}$$

where ρ is the liquid density, $\mathbf{u}$ is the liquid velocity, p denotes pressure, $v_{\text{eff}} = \upsilon + \upsilon_t$ is the effective kinematic viscosity as the sum of molecular and turbulent viscosity, $\mathbf{I}$ is the identity matrix, k the turbulent kinetic energy, and ε is the turbulent energy dissipation rate. The model coefficients $\sigma_k, \sigma_\varepsilon, C_{1\varepsilon,}$ and $C_{2\varepsilon}$ are 1.0, 1.2, 1.44, and 1.92, respectively, and G_k is the turbulence production term. The turbulent viscosity ν_t used in the calculation of the stress tensor is defined as $\nu_{\text{t}} = \rho C_{\mu} k^2/\varepsilon$ where C_{μ} is 0.09. The computational domain ends at the liquid surface, which is assumed to be flat.

Simulations are run for 20,000 iterations at which steady states is found to be achieved for all conditions based on a constant stirrer torque, average energy dissipation rate, and average velocity.

Based on the liquid results, bubble trajectories and residence times are analyzed by Lagrangian particle tracking

$$V_{\text{b}}\rho_{\text{g}}\frac{\partial \mathbf{v}}{\partial t} = \frac{3}{4}C_{\text{D}}V_{\text{b}}\frac{\rho}{d_{\text{b}}}(\mathbf{u}-\mathbf{v})|\mathbf{u}-\mathbf{v}| + V_{\text{b}}\mathbf{g}\left(\rho_{\text{g}}-\rho\right) + V_{\text{b}}\rho\frac{\text{D}\mathbf{u}}{\text{D}t} \tag{6}$$

where V_{b} is the bubble volume, d_{b} is the bubble diameter, ρ is the liquid density, ρ_{g} is the gas density, $\mathbf{v}$ is the bubble velocity, $\mathbf{g}$ is the gravitational acceleration, and D/D*t* denotes the substantial derivative. The first term on the right-hand side is the drag force, and the second and third terms are the gravitational and the pressure gradient force. The drag coefficient is calculated assuming bubbles behave like spherical particles [9].

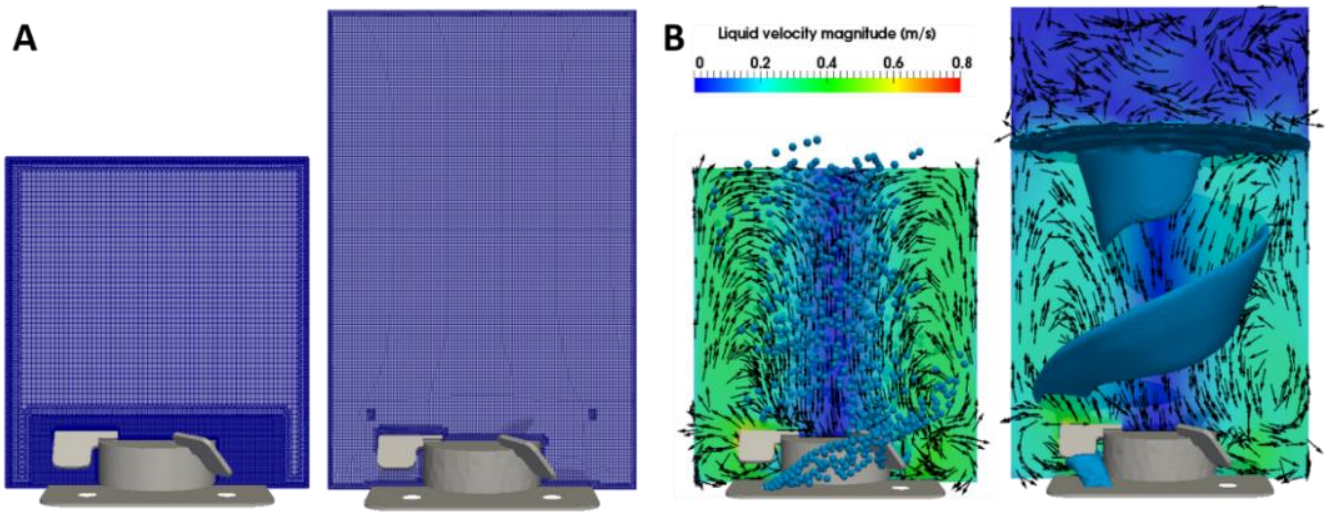

Fig. 1: **A:** Grids used for Euler-Lagrange simulations (left: 3.5 10^6 cells for 7 L volume) and for Euler-Euler simulations (right: 1.9 10^6 cells for the complete reactor). **B:** Euler-Lagrange (left) and Euler-Euler (right) liquid velocity for test condition 4; Euler-Lagrange bubble positions are indicate by spheres and for Euler-Euler, the 1 % gas volume fraction iso-surface is shown.

Euler-Euler simulations are performed with OpenFOAM v7 [10] using the reactingTwoPhaseEulerFoam solver. The interphase momentum transfer is included by a source term in the momentum equation. in Euler-Euler simulations turbulence is modeled with the mixture k-ε model [11]. Drag is described by the Schiller-Naumann equation [12]. Additionally, the virtual mass force $\mathbf{F}_{VM} = C_{\mathrm{VM}} V_{\mathrm{b}} \rho \left(\frac{\mathrm{D}\mathbf{u}}{\mathrm{D}t} - \frac{\mathrm{D}\mathbf{v}}{\mathrm{D}t}\right)$ is considered with a virtual mass coefficient C_{VM} of 0.5. Both phases can switch disperse and the continuous conditions for different regions of the computational domain. Thus, the domain can represent the complete reactor including the continuous gas in the head space. The simulations are run until quasi steady-state is achieved, i.e. when constant gas hold-up, volume-average liquid velocity, and stirrer torque are reached.

Grid generation is performed with the OpenFOAM [10] meshing tool snappyHexMesh. For Euler-Lagrange simulations, a separate grid for each working volume is created using the preconfigured settings of MixIT[8]. For OpenFOAM, a mesh of the complete domain is created and the working volume is defined by the initial condition of the gas volume fraction. For both approaches, grid independence has been tested with single phase steady state simulations (not shown) and the grids presented in Fig. 1 A are found to be sufficiently refined.

Simulation of mixing for both approaches is performed based on (quasi) steady-state results by solving for the convection of a passive tracer

$$\frac{\partial c}{\partial t} + \nabla(\alpha_{\mathrm{l}} \mathbf{u} c) = -\nabla(\alpha_{\mathrm{l}}(D_{\mathrm{m}} + \frac{\nu_{\mathrm{t}}}{\mathrm{Sc_t}})\nabla \mathrm{c}). \tag{7}$$

The tracer concentration c varies between zero and unity, and α_{L} is the liquid volume fraction. D_{m} is the molecular diffusivity of the tracer and $\frac{\nu_{\mathrm{t}}}{\mathrm{Sc_t}}$ represents the turbulent diffusivity, where the turbulent Schmidt number $\mathrm{Sc_t}$ is assumed to be 0.7. To determine the mixing time, the change in the tracer concentration is sampled at five different monitor positions distributed through the reactor, and mixing is considered to be achieved when the relative change in the tracer concentration at all monitor position is less than 0.005% between successive time steps.

Evaluation of the specific oxygen mass transfer coefficient $k_{\mathrm{L}}a$ from simulations is based on the eddy cell model of Lamont and Scott [13], where the transfer coefficient k_{L} is calculated according to

$$k_{\mathrm{L}} = c\sqrt{D_{\mathrm{O_2}}}\left(\frac{\varepsilon}{\nu}\right)^{0.25} \tag{8}$$

where D_{O_2} is the diffusion coefficient of oxygen in water ($3.0\ 10^{-9}$ m^2/s at 37° C [14]) and ν is the kinematic viscosity of the liquid.

For the Euler-Lagrange simulations, the overall gas hold-up $\alpha_{g,\mathrm{tot}}$ is calculated according to

$$\alpha_{\mathrm{g,tot}} = \frac{Q\ t_{\mathrm{r}}}{V} \tag{9}$$

where Q is the sparging rate, t_{r} is the average bubble residence time and V is the working volume. For Euler-Euler simulations, the gas volume fraction α_{G} in every control volume already is a simulation result. Based on the gas volume fraction and the bubble diameter d_{b}, the specific interface area a of spherical bubbles can be analyzed by

$$a = \frac{6\ \alpha_{\mathrm{g}}}{d_{\mathrm{b}}} \tag{10}$$

The $k_{\mathrm{L}}a$ is then determined as the product of the transfer coefficient k_{L} and specific interface area a

$$k_{\mathrm{L}}a = k_{\mathrm{L}}\ a \tag{11}$$

For Euler-Lagrange simulations, $k_{\mathrm{L}}a$ is evaluated for the average turbulent energy dissipation rate and bubble residence time, and for Euler-Euler simulations, this is done for every computational cell and the final value is determined as the volume average of the liquid-filled part of the domain for which is selected by a liquid volume fraction $\alpha_{\mathrm{l}} > 0.8$.

Evaluation of vortex formation for the Euler-Euler approach is analyzed from the air-liquid interface representation as the volume fraction iso-surface at $\alpha_{\mathrm{g}} = 1 - \alpha_{\mathrm{l}} = 0.5$. The vortex depth is determined as the maximum extension in vertical direction, and the increase of liquid height is determined relative to the initial liquid height. For Euler-Lagrange simulations

the observed pressure difference Δp between the wall and the center of the top boundary is assumed to correlate to the hydrostatic pressure difference that could be found between the lowest and highest liquid level of the vortex. Thus, the vortex depth Δh is calculated as $\Delta h = \frac{\Delta p}{\rho \mathbf{g}}$.

3. Results and Discussion

The results are presented and discussed in terms of different characteristics of the stirred tank bioreactor.

3.1 Liquid Velocity and Path of Bubble Rise

Liquid flow field results of the Euler-Lagrange and Euler-Euler simulation for condition 4 are given in Fig. 1 B. There is a dominant rotational motion due to the stirring. The secondary flow structure of radial and axial velocities shows two flow recirculation zones: a small recirculation zone resides below the stirrer blades with high velocity, and a second large recirculation zone with lower velocity is located above the stirrer blades. This pattern is found to be axisymmetric and is observed with both modeling approaches. Driven by buoyancy the bubbles rise in vertical direction. After their initial rise from the sparger below the stirrer blade, they briefly get captured behind the stirrer blades and detach again from the upper edge of the stirrer blades. After passing the stirrer, bubble rise is unimpeded in vertical direction. However, due to drag, bubbles are swept along with the liquid's rotational motion. The combination of vertical and rotational motion results in upward spiraling bubble trajectories in the center of the vessel, which can be seen in both modeling approaches.

3.2 Agitated Liquid Height and Vortex Formation

As the Xcellerex™ XDR-10 is an unbaffled reactor with a centered stirrer, vortex formation occurs at high stirrer speeds. In experiments, slight liquid surface deformation is found to appear at a stirrer speed of 100 rpm at all conditions with intermediate working volume (conditions 3 to 6), and more strongly, at the lowest working volume (condition 1), while for the maximum working volume no surface deformation is observed (condition 2). For the maximum stirrer speed at intermediate working volume (condition 8), clear vortex formation is found. This visual observation correlates well with the measured changes in agitated liquid height at the vessel wall. The same observation is made in the Euler-Euler simulations. Even though there are slight deviations in the absolute change of the liquid height, the trends are identical (see Table 2). The change in liquid height at the wall is relatively small compared to the total vortex depth, which is also found in Euler-Euler simulations. The vortex depth evaluated from Euler-Lagrange simulations also follows the same trend as the agitated liquid height and Euler-Euler simulation.

Table 2: Change in agitated liquid height observed in the experiment and predicted by Euler-Euler simulations, and vortex depth predicted by Euler-Euler simulations and on-way coupled Euler-Lagrange simulations for all test conditions defined in Table 1.

Condition number	Change in liquid height (mm)		Vortex depth (mm)	
	Experiment	Euler-Euler	Euler-Euler	Euler-Lagrange
1	4	2	10	15
2	0	0	1	1
3	3	1	8	12
4	3	1	8	12
5	3	1	8	12
6	3	1	8	12
7	0	0	0	1
8	28	44	145	229

3.3 Mixing Time and Oxygen Mass Transfer Coefficient

The experimentally observed range of mixing times is 3.6 s to 14.3 s, with short mixing times being found for the highest stirrer speed (condition 8) and the lowest working volume (condition 1). Long mixing times are observed for the lowest stirrer

speed (condition 7) and the maximum working volume (condition 2). The same observation is made with both simulation approaches shown in Fig. 2. For the intermediate levels of working volume and stirrer speed, intermediate mixing time is observed (conditions 3 to 6). The effect of sparging on the mixing time cannot be captured by one-way coupled Euler-Lagrange simulations, whereas the Euler-Euler simulations are able to capture the slight reduction of mixing time with increasing sparging rate (condition 3, 4 and 5). The experimentally observed range of $k_{\mathrm{L}}a$ is 0.9 h^{-1} to 19.9 h^{-1} where the lowest oxygen transfer rate occurs for the lowest sparging rate (condition 3). The center point condition 4 with intermediate sparging rate and impeller speed shows an intermediate oxygen transfer rate. High oxygen transfer rates are found for conditions 1, 8, and 5, which compared to condition 4 have a higher volumetric power input (conditions 1 and 8) or higher sparging rate (condition 5). For condition 8, the beneficial effect of volumetric power input is mitigated by the reduced bubble residence time due to vortex formation. The increase of $k_{\mathrm{L}}a$ with increasing sparging rate observed in experiments is also found in the simulations (condition 3, 4, and 5). Similarly, an increase in $k_{\mathrm{L}}a$ with stirrer speed is found when comparing conditions 7, 4, and 8. In contrast to expectations, the sparger with larger pore size, i.e. 20 µm for condition 6, does not show a reduced $k_{\mathrm{L}}a$, when compared to the sparger with smaller pore size, i.e. for the 2 µm sparger for condition 4. This might indicate that at the tested sparging rate, due to coalescence of bubbles formed at adjacent pores or single bubbles formed by to neighboring pores [15], the different mean pore size does not significantly alter the bubble Sauter mean diameter. A larger bubble size is assumed for the larger pore size sparger, and a smaller $k_{\mathrm{L}}a$ is predicted. The bubble size assumed is a critical input parameter. If it represents the actual bubble size distribution's Sauter mean diameter well, simulations should be able to accurately predict the available transfer area. However, bubble sizes are subject to change not only due to different sparger types, but also due to changes in operating conditions. This is one possible reason for the varying agreement to experimental $k_{\mathrm{L}}a$ data.

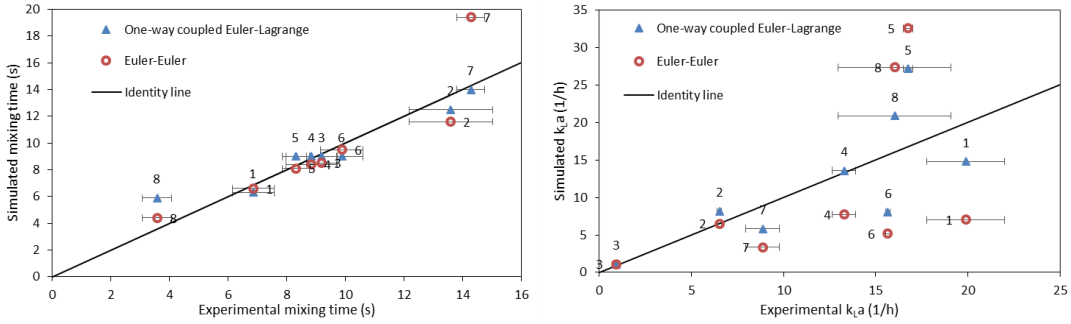

Fig. 2: Comparison of experimental and simulated mixing time and oxygen mass transfer ($k_{\mathrm{L}}a$): blue triangles (▲) represent Euler-Lagrange results, red circles (O) represent Euler-Euler results. The identity line is added for reference. Horizontal error bars represent the standard deviation of measurements taken in triplicate. Number labels indicate the test condition as defined in Table 1.

Table 3: Volume average turbulent kinetic energy dissipation rate and bubble residence time predicted for Euler-Lagrange and Euler-Euler simulation approaches.

Condition number	Average turbulent kinetic energy dissipation rate ε (m^2/s^3)		Average bubble residence time (s)	
	Euler-Lagrange	Euler-Euler	Euler-Lagrange	Euler-Euler
1	0.020	0.024	2.33	2.15
2	0.014	0.017	3.15	3.24
3	0.016	0.023	3.51	3.59
4		0.029		2.26
5		0.024		5.56
6		0.024	2.59	1.76
7	0.001	0.003	2.19	1.32
8	0.492	0.677	1.79	2.76

The decrease of $k_L a$ with increasing working volume for a constant stirrer speed (but reduced volumetric power input) is less pronounced in the simulations, where it is almost absent when comparing condition 1 and 4 (minimum and intermediate working volumes). As described in section 2, one important influencing factor for the prediction of $k_L a$ is the turbulent energy dissipation rate, which, following the eddy cell model of Lamont and Scott [13], heavily impacts the transfer coefficient k_L. The second important factor is the transfer area, which depends on the bubble surface area and residence time. Here, the bubble size has two effects: smaller bubbles have a higher surface area to volume ratio and a higher residence time which both result in a higher transfer area. Table 3 shows that for all conditions, the Euler-Euler approach predicts slightly higher energy dissipation rates than the Euler-Lagrange approach and for some conditions, significant deviation in the predicted residence times is found.

3.4 Risk of Cell Damage

Directly quantifying critical levels of hydrodynamic stress acting on the cultivated cells can be difficult without performing specialized measurements. An easily accessible parameter is the volumetric power input P/V which linearly correlates to the average energy dissipation rate. Sieck et al. [3] reported that already at an average energy dissipation rate of 0.4 m^2/s^3, negative effects on Chinese Hamster Ovary (CHO) cell productivity and transcriptomic stress responses could be observed. This level is exceeded for both simulation approaches for the maximum stirrer speed (condition 8). Using Euler-Euler simulation results for conditions 7, 4, and 8 to extrapolate average energy dissipation rate as a function of stirrer speed suggests an upper limit of stirrer speed of about 280 rpm to keep the average energy dissipation below the reported critical value [3]. When directly analyzing the effect of shear stress, Neunstoecklin et al. [5] have found the limit for CHO cells to be 32 Pa above which negative effects on productivity and product quality are observed. This maximum value is never observed for any condition in the present simulations (see Fig. 3). Furthermore, it can be observed that the maximum shear stress only depends on the impeller speed, which also determines the impeller tip speed and thus the maximum velocity inside the reactor.

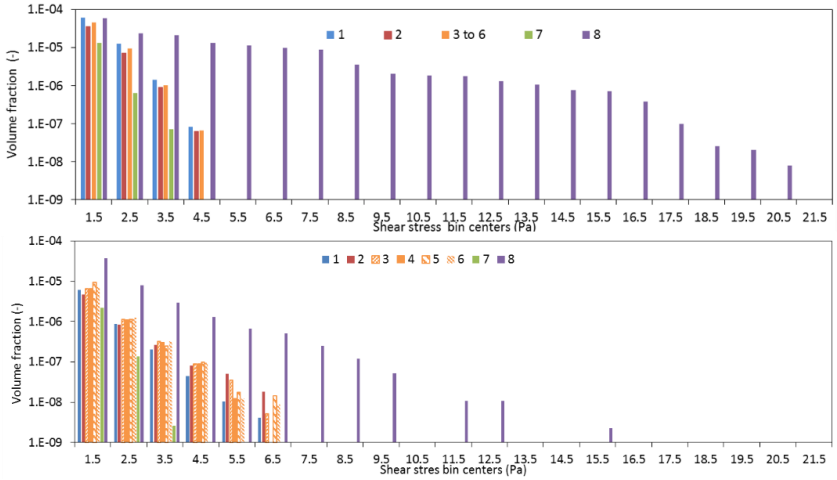

Fig. 3: Volume fraction of shear stress exceeding 1 Pa for the test conditions given in Table 1. Less than 0.1 % of total volume is represented for both Euler-Lagrange simulations (top) and Euler-Euler simulations (bottom).

4. Conclusions

Both the Euler-Euler and Euler-Lagrange models could successfully predict the effect of different operating conditions on the hydrodynamic characteristics of a single-use bioreactor. Vortex formation and mixing time are predicted accurately, and while oxygen mass transfer does only show limited agreement for some experimental conditions, the overall effects of changes in operating conditions are captured very well.

For the tested conditions, only the maximum stirrer speed of 360 rpm indicates possible cell damage due to high average energy dissipation. Increasing the stirrer speed to achieve an energy dissipation rate slightly below 0.4 m^2/s^3 (~ 280 rpm based on an extrapolation of the Euler-Euler simulation results) may be favorable as it allows for high oxygen transfer rates and

short mixing times. A negative effect of the increasing impeller speed is the increased vortex formation. This could be avoided if baffles were included or an angled stirrer instead of a centered stirrer was used. For the considered operating conditions, the effect of the gas bubbles on the liquid velocity is found to be small, and both the EL and the EE approaches give very similar results. Only the Euler-Euler simulations are able to directly predict vortex formation observed for the highest stirrer speed, while for the Euler-Lagrange simulations, vortex depth can be inferred from the pressure profile at the top boundary. Due to the significantly shorter simulation time, the one-way coupled Euler-Lagrange simulations appear preferable over the Euler-Euler simulations for a faster screening for a suitable range of operating conditions.

References

[1] R. Eibl, S. Kaiser, R. Lombriser, and D. Eibl, "Disposable bioreactors: the current state-of-the-art and recommended applications in biotechnology," *Applied Microbiology and Biotechnology,* vol. 86, no. 1, pp. 41-9, Mar 2010.

[2] S. Werner, S. C. Kaiser, M. Krause, and D. Eibel, "CFD as a modern tool for engineering characterization of bioreactors," *Pharmaceutical Bioprocessing,* vol. 2, no. 1, pp. 85-95, 2014.

[3] J. B. Sieck, T. Cordes, W. E. Budach, M. H. Rhiel, Z. Suemeghy, C. Leist, T. K. Villiger, M. Morbidelli, and M. Soos, "Development of a Scale-Down Model of hydrodynamic stress to study the performance of an industrial CHO cell line under simulated production scale bioreactor conditions," *Journal of Biotechnology,* vol. 164, no. 1, pp. 41-9, Mar 10 2013.

[4] S. Wollny, "Experimentelle und numerische Untersuchungen zur Partikelbeanspruchung in gerührten (Bio-)Reaktoren," Ph. D., Fakultät III-Prozesswissenschaften, Technischen Universität Berlin, Berlin, 2010.

[5] B. Neunstoecklin, M. Stettler, T. Solacroup, H. Broly, M. Morbidelli, and M. Soos, "Determination of the maximum operating range of hydrodynamic stress in mammalian cell culture," *Journal of Biotechnology,* vol. 194, pp. 100-9, Jan 20 2015.

[6] C. Löffelholz, U. Husemann, G. Greller, W. Meusel, J. Kauling, P. Ay, M. Kraume, R. Eibl, and D. Eibl, "Bioengineering Parameters for Single-Use Bioreactors: Overview and Evaluation of Suitable Methods," *Chemie Ingenieur Technik,* vol. 85, no. 1-2, pp. 40-56, 2013.

[7] F. Garcia-Ochoa and E. Gomez, "Bioreactor scale-up and oxygen transfer rate in microbial processes: an overview," *Biotechnology Advances,* vol. 27, no. 2, pp. 153-76, Mar-Apr 2009.

[8] MixIT. (2019). *https://tridiagonal.com/mixit/*.

[9] A. A. Amsden, T. D. Butler, and P. J. O'Rourke, "The KIVA-II computer program for transient multidimensional chemically reactive flows with sprays," in "SAE Technical Paper," Los Alamos National Lab. (LANL), Los Alamos, NM (United States)1987.

[10] OpenFOAM. (2019). *www.openfoam.org*.

[11] A. Behzadi, R. I. Issa, and H. Rusche, "Modelling of dispersed bubble and droplet flow at high phase fractions," *Chemical Engineering Science,* vol. 59, no. 4, pp. 759-770, 2004.

[12] L. Schiller and A. Z. Neumann, " A drag coefficient correlation," *VDI Zeitschrift,* vol. 77, 1933.

[13] J. C. Lamont and D. S. Scott, "An Eddy Cell Model of Mass Transfer into the Surface of a Turbulent Liquid," *AIChE Journal,* vol. 16, no. 4, 1970.

[14] P. Han and D. M. Bartels, "Temperature Dependence of Oxygen Diffusion in H2O and D2O," *The Journal of Chemical Physics,* vol. 100, pp. 5997-5602, 1996.

[15] N.A. Kazakis, A.A. Mouza, and S. V. Paras, "Experimental study of bubble formation at metal porous spargers: Effect of liquid properties and sparger characteristics on the initial bubble size distribution," *Chemical Engineering Journal,* vol. 137, pp. 265–281, 2008.